Cardiovascular Research (2013) **99**, 442–451
doi:10.1093/cvr/cvt124

# Early structural and metabolic cardiac remodelling in response to inducible adipose triglyceride lipase ablation

**Petra C. Kienesberger[1,2†‡], Thomas Pulinilkunnil[1,2†‡], Jeevan Nagendran[1,3], Martin E. Young[4], Juliane G. Bogner-Strauss[5], Hubert Hackl[6], Rammy Khadour[1,2], Emma Heydari[1,2], Guenter Haemmerle[7], Rudolf Zechner[7], Erin E. Kershaw[8*], and Jason R. B. Dyck[1,2,9*]**

[1]Cardiovascular Research Centre, Mazankowski Alberta Heart Institute, University of Alberta, Edmonton, AB, Canada T6G 2S2; [2]Department of Pediatrics, University of Alberta, Edmonton, AB, Canada T6G 2S2; [3]Department of Medicine, Faculty of Medicine and Dentistry, University of Alberta, Edmonton, AB, Canada T6G 2S2; [4]Department of Medicine, University of Alabama at Birmingham, Birmingham, AL 35294, USA; [5]Institute for Genomics and Bioinformatics, Graz University of Technology, 8010 Graz, Austria; [6]Biocenter, Division of Bioinformatics, Innsbruck Medical University, 6020 Innsbruck, Austria; [7]Institute of Molecular Biosciences, University of Graz, 8010 Graz, Austria; [8]Division of Endocrinology and Metabolism, Department of Medicine, University of Pittsburgh, 200 Lothrop Street, BST E1140 Pittsburgh, PA 15261, USA; and [9]458 Heritage Medical Research Centre, University of Alberta, 112 Street & 87 Avenue, Edmonton, Alberta, Canada T6G 2S2

*Received 19 January 2013; revised 28 April 2013; accepted 9 May 2013; online publish-ahead-of-print 25 May 2013*

**Time for primary review: 41 days**

**Aims** While chronic alterations in cardiac triacylglycerol (TAG) metabolism and accumulation are associated with cardiomyopathy, it is unclear whether TAG catabolizing enzymes such as adipose triglyceride lipase (ATGL) play a role in acquired cardiomyopathies. Importantly, germline deletion of ATGL leads to marked cardiac steatosis and heart failure in part through reducing peroxisome proliferator-activated receptor α (PPARα) activity and subsequent fatty acid oxidation (FAO). However, whether ATGL deficiency specifically in adult cardiomyocytes contributes to impaired PPARα activity, cardiac function, and metabolism is not known.

**Methods and results** To study the effects of acquired cardiac ATGL deficiency on cardiac PPARα activity, function, and metabolism, we generated adult mice with tamoxifen-inducible cardiomyocyte-specific ATGL deficiency (ic*Atgl*KO). Within 4–6 weeks following ATGL ablation, ic*Atgl*KO mice had markedly increased myocardial TAG accumulation, fibrotic remodelling, and pathological hypertrophy. Echocardiographic analysis of hearts *in vivo* revealed that contractile function was moderately reduced in ic*Atgl*KO mice. Analysis of energy metabolism in e*x vivo* perfused working hearts showed diminished FAO rates which was not paralleled by markedly impaired PPARα target gene expression.

**Conclusions** This study shows that acquired cardiomyocyte-specific ATGL deficiency in adult mice is sufficient to promote fibrotic and hypertrophic cardiomyopathy and impair myocardial FAO in the absence of markedly reduced PPARα signalling.

**Keywords** Cardiomyopathy • Lipid metabolism • Lipid signalling • Remodelling • ATGL

## 1. Introduction

Under physiological conditions, the heart relies primarily on mitochondrial fatty acid (FA) oxidation (FAO) for ATP production.[1] Upon entry into the cardiomyocyte, FAs that are not immediately oxidized are esterified to triacylglycerol (TAG) and stored in cytosolic lipid droplets.[2] However, chronically increased myocardial TAG content (i.e. myocardial steatosis) observed in certain diseases is associated with cardiomyopathy in both rodents and humans.[3–9] Having said that, it is unlikely that intramyocardial TAGs *per se* directly cause cardiomyocyte dysfunction.[10–15] Instead, it is more probable that changes in TAG metabolism indirectly contribute to cardiac dysfunction by influencing myocardial

† These authors contributed equally.

‡ Present address: Dalhousie Medicine New Brunswick, Department of Biochemistry and Molecular Biology, Dalhousie University, E2L 4L5 Saint John, New Brunswick, Canada.

* Corresponding authors. Tel: +1 4126489770; fax: +1 4126483290, Email: kershawe@pitt.edu (E.E.K.). Tel: +1 7804920314; fax: +1 7804929753, Email: jason.dyck@ualberta.ca (J.R.B.D).

accumulation of lipotoxic FA metabolites, such as ceramides, diacylglycerols, long-chain acyl-CoAs, or acylcarnitines. Previous work has identified adipose triglyceride lipase (ATGL) as rate limiting for cytosolic TAG hydrolysis in many tissues.[16] The importance of ATGL action in the heart is supported by the observation that patients with mutations in the *ATGL* gene (*PNPLA2*) exhibit myocardial steatosis and cardiomyopathy.[17–21] Increased myocardial TAG accumulation is associated with cardiomyopathy in humans during conditions such as obesity, insulin resistance, diabetes mellitus, and ageing,[3,9,22–27] suggesting that alterations in myocardial TAG metabolism and specifically ATGL may also play a role in acquired human cardiomyopathies.

Similar to humans with (inactivating) *ATGL* mutations, mice with constitutive whole body ATGL deficiency (total*Atgl*KO) showed markedly increased myocardial TAG accumulation, which was associated with reduced peroxisome proliferator-activated receptor α (PPARα) activity, leading to mitochondrial dysfunction and lethal cardiomyopathy.[28] These data suggest that myocardial ATGL is crucial for PPARα activation and mitochondrial function.[28] In addition to these metabolic derangements, total*Atgl*KO mice also presented with cardiac fibrosis and increased ventricular wall dimensions.[16,28] However, since whole body ATGL deficiency results in potentially confounding effects such as reduced serum lipid levels, altered concentrations of circulating adipokines, and impaired insulin secretion,[16,29] as well as developmental adaptations due to germline ATGL deficiency, it is not clear whether acquired cardiac ATGL deficiency in the adult cardiomyocyte would recapitulate the cardiac metabolic phenotype observed in the total*Atgl*KO mice. In addition, it is unknown whether cardiac fibrosis in total*Atgl*KO mice was a direct effect of ATGL deficiency in cardiac fibroblasts.

The aim of this study was to determine whether short term, acquired ATGL deficiency in adult cardiomyocytes contributes to impaired cardiac function, metabolism, and remodelling.

# 2. Methods

An expanded Methods section is available in the Supplementary material online.

## 2.1 Generation of the *Atgl/Pnpla2-loxP* targeting construct and ic*Atgl*KO mice

Mice carrying a LoxP-modified *Atgl* allele (B6.129-*Pnpla2*$^{tm1Eek}$ mice; herein designated as *Atgl*-flox mice) were generated in the laboratory of Erin Kershaw using BAC recombineering. *Atgl*-flox mice [backcrossed onto the C57BL/6NTac (Taconic) background for more than four generations] were interbred with B6.Cg-Tg(Myh6-cre/Esr1)1Jmk/J mice (#005657, The Jackson Laboratory, backcrossed onto the C57BL/6J background for >10 generations), which express a tamoxifen-inducible Cre recombinase driven by the cardiomyocyte-specific α-myosin heavy chain promoter (offspring are estimated to have >96.9% C57BL/6 background). The C57BL/6J, but not C57BL/6NTac subline harbours a mutation in the gene encoding nicotinamide nucleotide transhydrogenase, which promotes antioxidant capacity in mitochondria and is expressed in the heart.[30] Control and ic*Atgl*KO mice were derived from the same breeder pairs to avoid confounding effects due to differences in genetic background. Tamoxifen (#T5648, Sigma) dissolved in corn oil was administered orally to adult control (homozygous *Atgl*-flox without Cre, *Atgl*$^{flox/flox}$ −/−) and inducible cardiomyocyte-specific ATGL knockout (ic*Atgl*KO; homozygous *Atgl*-flox and hemizygous for Cre, *Atgl*$^{flox/flox}$ Cre/−) mice at a dose of 80 mg/kg/day for six consecutive days. Mice were housed on a 12 h light:12 h dark cycle with *ad libitum* access to chow diet (#5001 from Lab Diet with 13.5% kcal from fat) and water. Unless otherwise stated, non-fasted mice were used and euthanasia was performed by decapitation. All protocols involving mice were approved by the University of Alberta Institutional Animal Care and Use Committee and conform with the *Guide for the Care and Use of Laboratory Animals* published by the United States National Institutes of Health.

## 2.2 Analysis of serum insulin, lipids, and lactate

Serum insulin was determined using the mouse insulin enzyme-linked immunosorbent assay kit (#90080, Crystal Chem). Serum free fatty acids (FFA) and TAGs were determined using colorimetric kit assays [#HR Series NEFA-HR(2), Wako and #2780−400H Infinity TAG reagent, Thermo Electron]. Serum lactate was determined using a fluorometric kit assay (#700510, Cayman).

## 2.3 Echocardiography

Mice were mildly anaesthetized using 0.75% isoflurane, and transthoracic echocardiography was performed as described previously.[31]

## 2.4 Heart perfusions

Hearts were perfused aerobically in working mode with Krebs−Henseleit buffer containing 0.8 mmol/L oleate prebound to 3% delipidated bovine serum albumin, 5 mmol/L glucose, and 50 μU/mL insulin for 60 min as described previously.[31]

## 2.5 Cardiomyocyte isolation

Ventricular calcium-tolerant myocytes were isolated from Langendorff perfused hearts similar to a previously described procedure.[32]

## 2.6 Tissue homogenization and lipid analysis

Tissues were homogenized as described previously.[31] Lipids were isolated from homogenates, followed by the colorimetric determination of TAG concentrations. To examine oleate incorporation into TAGs from perfused hearts, TAGs were isolated by thin layer chromatography, and labelled oleate was measured by liquid scintillation counting.

## 2.7 Immunoblot analysis

Tissue lysates were resolved by SDS−PAGE and immunoblot analysis was performed as described previously.[31]

## 2.8 Mitochondrial enzyme activities and ATP production

Citrate synthase and β-hydroxyacyl-CoA dehydrogenase (HADH) activity in ventricular homogenates was assessed spectrophotometrically according to Boudina *et al.*[33] with modifications. ATP synthesis rates in freshly isolated mitochondria were measured using a bioluminescence-based method employing firefly luciferase.[34]

## 2.9 Gene expression

Gene expression analysis was performed by quantitative reverse transcriptase PCR as previously described[35] (see Supplementary material online, *Table S1*).

## 2.10 Microarray analysis

Total RNA was isolated from frozen ventricular tissue using TRIzol reagent (Invitrogen), and microarray analysis was performed as described previously[36] with modifications. Differentially expressed genes were identified using the moderated *t*-test with the R/Bioconductor package limma. Multiple hypothesis testing was considered according to the method of Benjamini and Hochberg.[37]

## 2.11 Histology

Haematoxylin and eosin (H&E) and Masson's trichrome (M.T.) stains of paraffin-embedded sections were visualized as described previously.[31]

### 2.12 Electron microscopy and mitochondrial morphometry

Electron microscopy was performed as previously described.[38] Intermyofibrillar mitochondria, which were entirely included in the field of view, were quantified from images at 7100-fold magnification. Mitochondrial cross-sectional area and minimum and maximum Feret's diameter were determined using ImageJ software (National Institutes of Health).

### 2.13 Statistical analysis

Results are expressed as means ± SEM. Comparisons between groups were made by the unpaired two-tailed Student *t* test using the GraphPad Prism software, unless otherwise stated. *P*-values of $<0.05$ were considered statistically significant.

## 3. Results

### 3.1 Inducible cardiomyocyte-specific ATGL deficiency results in myocardial steatosis and fibrotic remodelling

ATGL protein expression was diminished in ventricles and isolated cardiomyocytes from ic*Atgl*KO mice compared with control mice (*Figure 1A*), confirming ablation of ATGL protein. Cardiomyocytes isolated from ic*Atgl*KO mice also exhibited a drastically altered morphology with large vacuoles (*Figure 1B*). Similar to previous observations in total*Atgl*KO and striated muscle-specific ATGL knockout (muscle*Atgl*KO) mice,[28] the cardiac TAG content was markedly increased in ic*Atgl*KO mice (*Figures 1C, D* and *5D*). Serum concentrations of FFA, TAGs, insulin, and lactate were unchanged between genotypes (*Figure 1E–H*). These findings show that ATGL specifically in cardiomyocytes is rate limiting for myocardial TAG catabolism.

Histological analysis showed significantly altered tissue morphology in hearts from ic*Atgl*KO mice, which was characterized by accumulation of vacuoles as well as interstitial fibrosis (*Figure 1I*) (15.53 ± 0.51% fibrosis area in ic*Atgl*KO compared with none in control hearts, averages of two to three images per heart × 3 hearts per group). Fibrotic remodelling in hearts from ic*Atgl*KO mice also corresponded with increased collagen (*Col1a1*) and transforming growth factor β (*Tgfb*) mRNA expression (*Figure 1J*). In addition, microarray analysis showed up-regulation of numerous genes involved in extracellular matrix remodelling in hearts from ic*Atgl*KO mice, including periostin (*Postn*), kallikrein-related peptidase 7 (*Klk7*), collagen type I (*Col1a1* and *Col1a2*) and III (*Col3a1*), reticulon 4 (Nogo, *Rtn4*), CD44 antigen (*CD44*), chemokine (C-C motif) receptor 2/5 (*Ccr2*/*Ccr5*), decorin (*Dcn*), and galectin-3 (*Lgals3*) (*Figure 2A*). Together, these findings suggest that ic*Atgl*KO mice develop rapid fibrotic myocardial remodelling in parallel with cardiac steatosis.

Protein expression of the apoptosis markers, phospho-P38 mitogen-activated protein kinase (MAPK) (Thr180/Tyr182), and phospho-c-Jun-amino-terminal kinase (JNK) (Thr183/Tyr185) was comparable between hearts from ic*Atgl*KO and control mice (*Figure 2B* and *C*), although expression of cleaved Poly(ADP-Ribose) Polymerase (PARP) trended to increase in hearts from ic*Atgl*KO mice (*Figure 2D*). These data indicate the absence of marked induction of apoptosis following short-term ATGL ablation and are consistent with low levels of apoptosis in hearts from total*Atgl*KO mice.[16]

### 3.2 Inducible cardiomyocyte-specific ATGL deficiency leads to moderate *in vivo* cardiac dysfunction

Examination of *in vivo* cardiac function using transthoracic echocardiography revealed that ejection fraction and fractional shortening were reduced by 15 and 18%, respectively, in hearts from ic*Atgl*KO mice (*Figure 3A–C*), which also corresponded with reduced peak systolic mitral annular velocity (S′) (*Table 1*). Despite unchanged diastolic parameters such as the ratio of early (E) to late (A) transmitral filling velocity (*Figure 3D*), mitral valve deceleration time (*Figure 3E*), and isovolumic relaxation time (*Figure 3F*), early and late diastolic mitral annular velocity (E′ and A′, respectively) (*Figure 3G*, *Table 1*) were decreased in hearts from ic*Atgl*KO mice with concomitantly increased ratio of E to E′ (*Figure 3H*), indicating elevated left ventricular filling pressure in ic*Atgl*KO mice. Together, these data suggest that ic*Atgl*KO mice exhibit modest cardiac dysfunction *in vivo*.

### 3.3 Inducible cardiomyocyte-specific ATGL deficiency leads to hypertrophy

Since hearts from ic*Atgl*KO mice are so lipid laden, we tested whether true hypertrophic remodelling contributes to the enlarged appearance of cardiomyocytes and hearts from ic*Atgl*KO mice (*Figure 1B* and *C*). The ventricle weight-to-tibia length ratio (*Figure 4A*) and the left ventricular mass as assessed by echocardiography (*Table 1*) were significantly increased in ic*Atgl*KO mice compared with controls. Histological images of long-axis heart sections also showed increased ventricle wall thickness in ic*Atgl*KO mice (*Figure 4B*). Assessment of ventricular wall dimensions and left ventricular internal diameters in diastole and systole (LVIDd and LVIDs, respectively) using echocardiography confirmed increased thickness of the interventricular septum and left ventricular posterior wall in ic*Atgl*KO mice in the absence of ventricular dilatation (*Figure 4C* and *D*, *Table 1*). Most importantly, transcript levels of brain natriuretic peptide (*Nppb*) and beta myosin heavy chain (*Myh7*), which are marker genes for pathological hypertrophy, were correspondingly up-regulated in hearts from ic*Atgl*KO mice (*Figure 4E*). In accordance with this finding, microarray analysis showed up-regulation of several genes involved in pathological hypertrophic growth, such as signal transducer and activator of transcription 5A (*Stat5a*), follistatin-like 1 (*Fstl1*), and β-catenin (*Ctnnb1*) (*Figure 2A*). In addition, phosphorylation and protein expression of STAT3, which is also an indicator of cardiac hypertrophy, was increased in hearts from ic*Atgl*KO mice (*Figure 4F*). In contrast, protein expression of catalase (*Figure 4G*), manganese superoxide dismutase (MnSOD) (*Figure 4H*), and 4-hydroxy-2-nonenal (4-HNE) Michael adducts (*Figure 4I*; $n = 5–6$, $P = 0.96$) was not increased in hearts from ic*Atgl*KO mice, suggesting that hypertrophic and fibrotic remodelling of the myocardium is not due to increased oxidative stress in ic*Atgl*KO mice. Taken together, these findings suggest that ic*Atgl*KO mice develop overt hypertrophic remodelling in the absence of increased oxidative stress.

### 3.4 Inducible cardiomyocyte-specific ATGL deficiency results in diminished myocardial FAO

We determined FA and glucose oxidation rates in *ex vivo* perfused working hearts using radiolabelled substrates. *Ex vivo* cardiac power

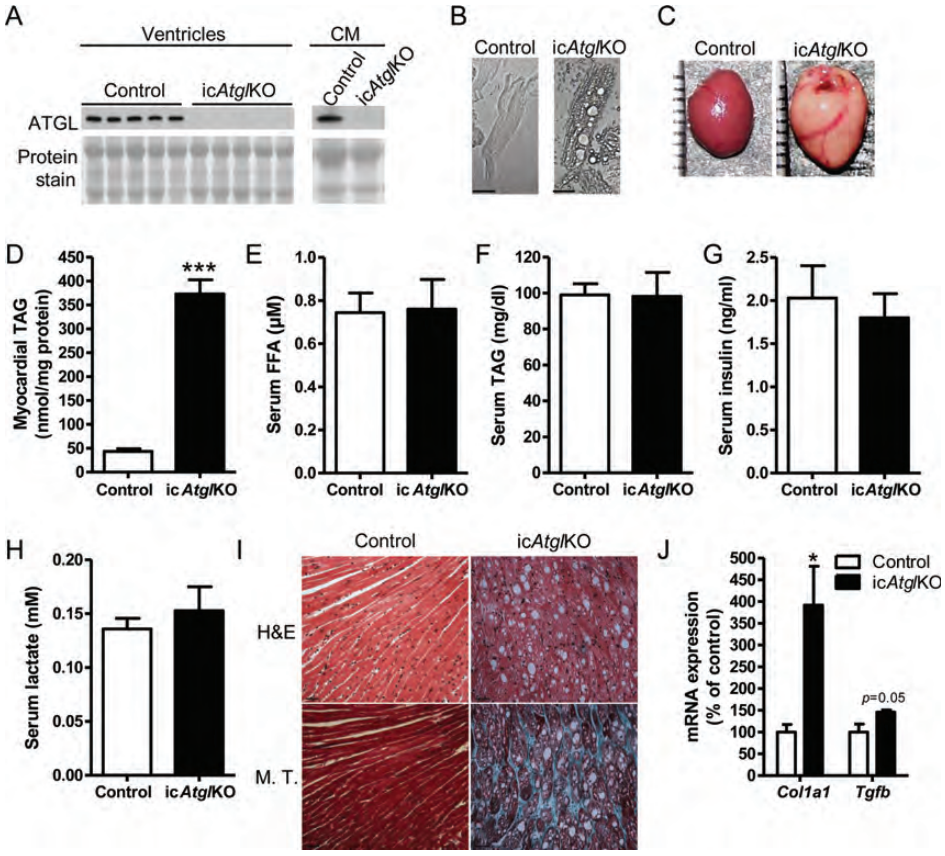


**Figure 1** Cardiac morphology, myocardial TAG content, and serum analysis. (*A*) Cardiac ATGL protein expression (4 weeks *post*-TAM, 6–7-month-old females) and isolated cardiomyocytes (CM) (4 weeks *post*-TAM, 11.5-month-old males). (*B*) Representative light microscopy images of isolated cardiomyocytes at ×400 magnification (6 weeks *post*-TAM, 7.5-month-old males). Scale bars denote 30 μm. (*C*) Representative images of isolated hearts (5 weeks *post*-TAM, 5–6-month-old males). (*D*) Myocardial TAG content (5 weeks *post*-TAM, 5–6-month-old males, $n = 5$, $^{***}P < 0.0001$). (*E*) Serum FFA (5 weeks *post*-TAM, 5–6-month-old males, $n = 5$), (*F*) TAGs (5 weeks *post*-TAM, 5–6-month-old males, $n = 5$), (*G*) insulin (5 weeks *post*-TAM, 5–6-month-old males, $n = 5$), and (*H*) lactate (4 week *post*-TAM, 4–7-month-old females, $n = 6$). (*I*) Representative histological images of apical heart sections (5 weeks *post*-TAM, 5–6-month-old males) stained with H&E and M.T. stain at ×400 magnification. Scale bars denote 30 μm. (*J*) Cardiac mRNA expression of *Col1a1* and *Tgfb* (5 weeks *post*-TAM, 5–6-month-old males, $n = 4–5$, $^{*}P < 0.05$).

was comparable between genotypes (see Supplementary material online, *Figure S2A*), but was reduced in hearts from ic*Atgl*KO mice when normalized to cardiac dry weight (*Figure 5A*). Oleate oxidation rates were decreased in hearts from ic*Atgl*KO mice compared with controls (*Figure 5B*, see Supplementary material online, *Figure S2B*), which was not associated with a compensatory increase in glucose oxidation rates (*Figure 5C*, see Supplementary material online, *Figure S2C*). Incorporation of oleate into the TAG pool was decreased in hearts from ic*Atgl*KO mice (*Figure 5E*), suggesting that enhanced sequestration of labelled oleate in TAGs does not confound oleate oxidation rates measured in these hearts. Interestingly, reduced FAO and FA incorporation into TAGs were also associated with decreased protein expression of the FA translocase, CD36, but not FATP1 (*Figure 5G*). In addition, the activity of the FAO enzyme, HADH, was also decreased in hearts from ic*Atgl*KO mice (*Figure 5F*). Together, these data suggest that reduced myocardial FAO likely contributes to the cardiac contractile dysfunction *in vivo* in ic*Atgl*KO mice.

## 3.5 Inducible cardiomyocyte-specific ATGL deficiency does not dramatically impair PPARα activity

Contrary to our expectations, we found that PPARα protein expression was increased in hearts from ic*Atgl*KO mice (*Figure 5H*) and that mRNA expression of PPARα (*Ppara*) and the PPARα target genes, 1-acylglycerol-3-phosphate O-acyltransferase 3 (*Agpat3*), pyruvate dehydrogenase kinase isozyme 4 (*Pdk4*), medium-chain acyl-CoA dehydrogenase (*Mcad*), and mitochondrial acyl-CoA thioesterase 1 (*Mte1*) was unimpaired in hearts from non-fasted ic*Atgl*KO mice (*Figure 5I*). In addition, mRNA expression of diacylglycerol *O*-acyltransferase 2 (*Dgat2*) and glucose transporter type 1 (*Glut1*) was also unchanged in hearts from ic*Atgl*KO mice (*Figure 5I*). Microarray analysis likewise showed no significant changes in the expression of PPARα, PPARα target genes, and other genes involved in FA utilization (data not shown). However, a relatively moderate reduction in the mRNA expression of some PPARα target genes was

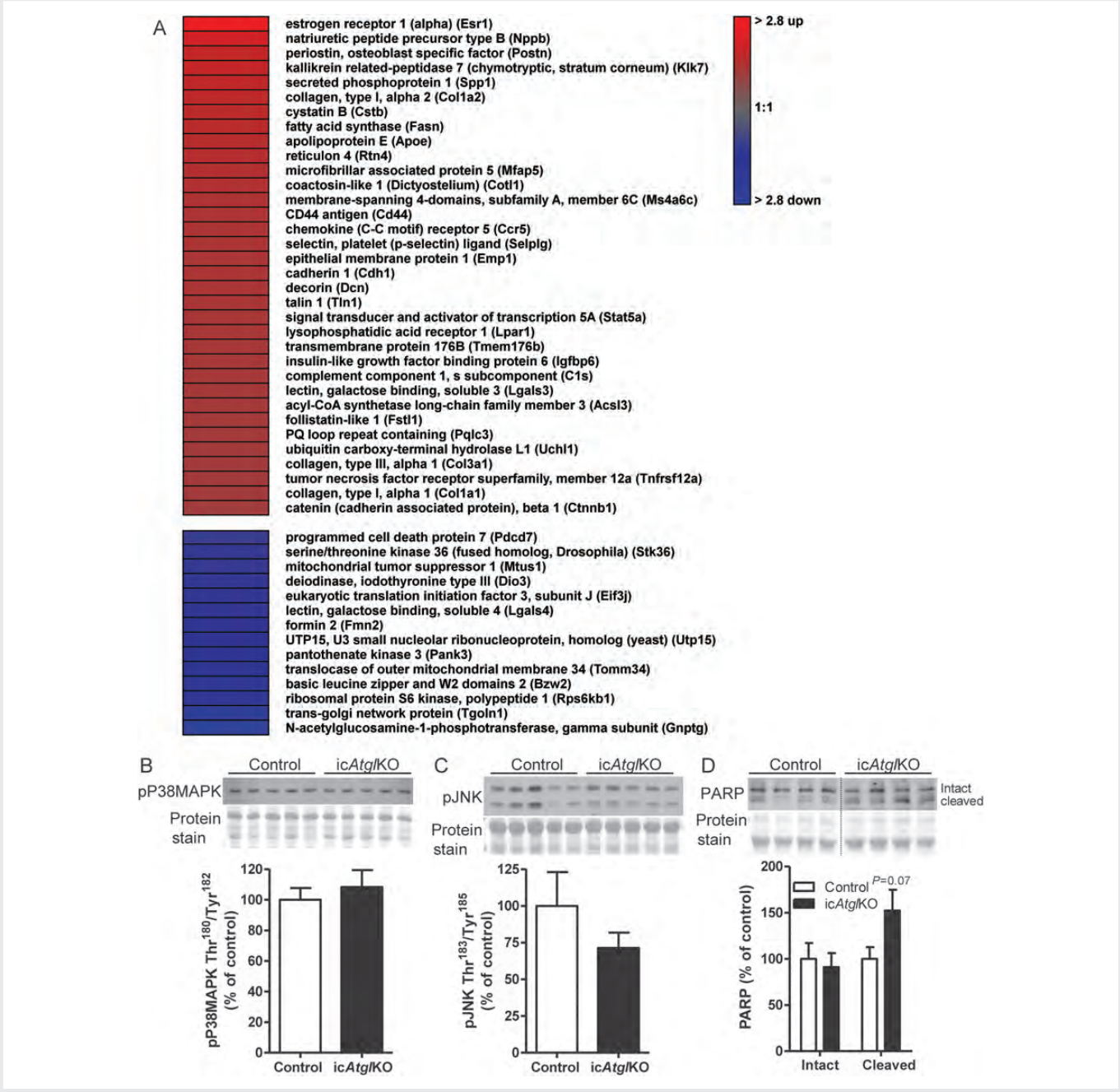


**Figure 2** Microarray analysis and markers of apoptosis. (*A*) Heat map of differentially regulated genes (fold change $\geq$ 1.5, $P < 0.05$) comparing hearts from 5 h-fasted ic*Atgl*KO vs. control mice (5.5 weeks *post*-TAM, 5–8-month-old females, $n = 3$) as assessed by microarray analysis. (*B*) Cardiac protein expression of P38MAPK phosphorylated at Thr180/Tyr182 and (*C*) JNK phosphorylated at Thr183/Tyr185 (4 weeks *post*-TAM, 6-month-old females, $n = 5–6$). (*D*) Cardiac protein expression of PARP (4 weeks *post*-TAM, 5–6-month-old females, $n = 4–5$).

observed in hearts from ic*Atgl*KO mice following prolonged (12 h) fasting (*Figure 5J*). These findings suggest that PPARα target gene expression is not significantly impaired in hearts from ic*Atgl*KO mice in the non-fasted and short-term fasted state, but may become more physiologically relevant during prolonged fasting. Interestingly, hormone-sensitive lipase (HSL) phosphorylation at Ser660 was increased in hearts from ic*Atgl*KO mice (*Figure 5K*), suggestive of enhanced HSL activation that may contribute to sustained PPARα target gene expression.

To determine the impact of inducible cardiomyocyte-specific ATGL deficiency on mitochondria directly, we assessed multiple mitochondrial parameters. Inspection of myocardial tissue morphology by transmission electron microscopy revealed dramatically enlarged lipid droplets in the intermyofibrillar space in proximity to mitochondria (*Figure 6A*). However, no clear differences were noted between genotypes for mitochondria shape or ultrastructural characteristics (*Figure 6A*). More objective quantification of mitochondrial number (*Figure 6B*) as well as individual mitochondrial area (*Figure 6D*) and diameter (*Figure 6E* and *F*) revealed that these parameters did not differ between genotypes. In addition, citrate synthase activity (*Figure 6C*), a surrogate measure of both mitochondrial mass and Krebs cycle activity, was similar between

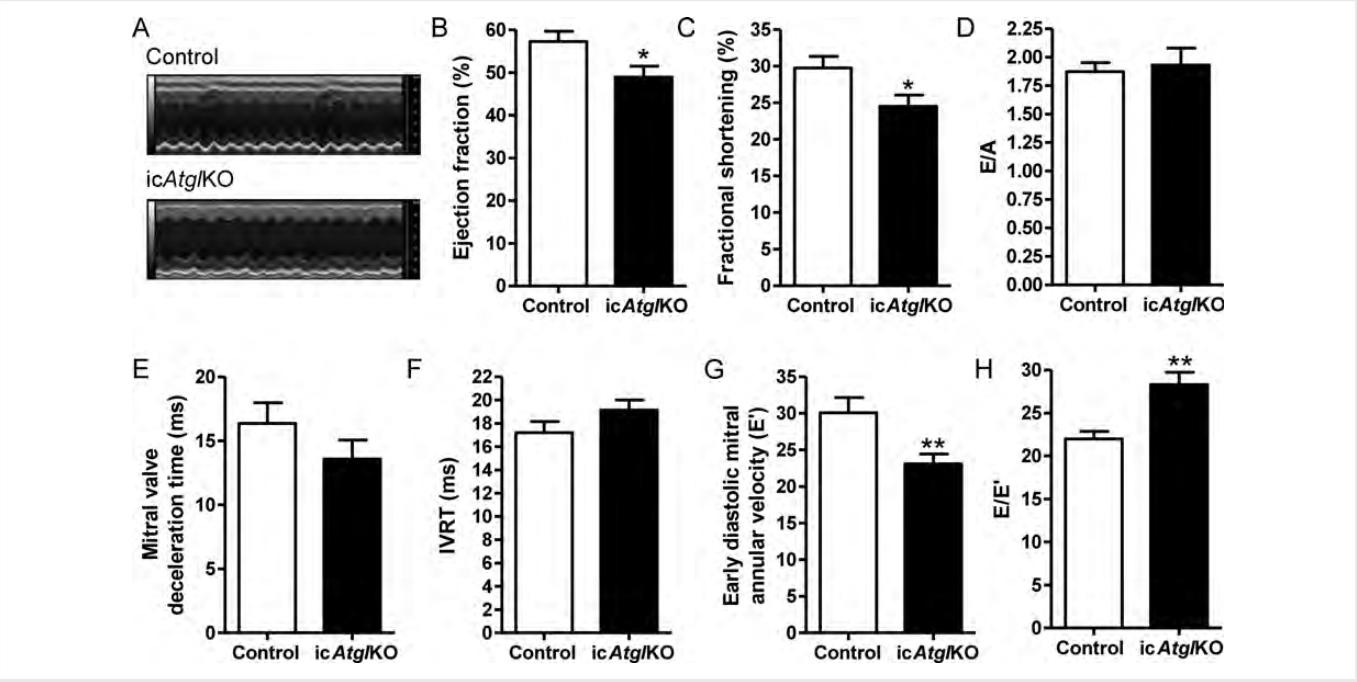


**Figure 3** *In vivo* cardiac function. (*A*–*H*) Functional parameters obtained by transthoracic echocardiography (4 weeks *post*-TAM, 3–6-month-old females, $n = 8–13$, $^{*}P < 0.05$, $^{**}P < 0.01$). Cardiac function was similar within this age group. (*A*) Representative M-mode images. (*B*) Ejection fraction. (*C*) Fractional shortening. (*D*) Ratio of E to A. (*E*) Mitral valve deceleration time. (*F*) Isovolumic relaxation time. (*G*) E'. (*H*) Ratio of E to E'.

**Table 1 Body weight and *in vivo* heart function of anaesthetized control and ic*Atgl*KO mice**

| | Control | ic*Atgl*KO |
|---|---|---|
| Body weight (g) | 24.4 ± 0.9 | 22.9 ± 0.7 |
| Heart rate (b.p.m.) | 426 ± 12 | 416 ± 11 |
| Left ventricular mass (mg) | 69.2 ± 2.8 | 90.2 ± 3.6‡ |
| LVIDd (mm) | 3.85 ± 0.04 | 3.80 ± 0.05 |
| LVIDs (mm) | 2.71 ± 0.07 | 2.88 ± 0.09 |
| IVSs (mm) | 0.97 ± 0.04 | 1.1 ± 0.02† |
| LVPWs (mm) | 0.97 ± 0.03 | 1.08 ± 0.02† |
| Ejection time (ms) | 49.8 ± 1.0 | 48.4 ± 1.2 |
| IVCT (ms) | 19.0 ± 0.9 | 19.0 ± 1.2 |
| Mitral E (mm/s) | 654 ± 41 | 634 ± 21 |
| E′/A′ | 1.13 ± 0.08 | 1.17 ± 0.04 |
| A′ (cm/s) | 26.8 ± 0.9 | 20.1 ± 1.4† |
| S′ (cm/s) | 21.5 ± 0.9 | 17.2 ± 1.0† |

4 weeks *post*-TAM, 3–6 month-old females, $n = 8–13$.
†$P < 0.01$.
‡$P < 0.001$.

genotypes. ATP production rates via complex I (pyruvate/malate) were not significantly different between genotypes, but were reduced via complex II (succinate/rotenone) and IV (TMPD/ascorbate) as well as in the absence of exogenous substrate (ADP only) in ic*Atgl*KO mitochondria (*Figure 6G*). Together, these data suggest that inducible cardiomyocyte-specific ATGL deficiency does not significantly impact mitochondrial morphology or mass, but impairs mitochondrial function at the level of ATP synthesis. Moreover, hearts from ic*Atgl*KO mice displayed areas of myofibrillar disarray (*Figure 6A*), which may contribute to hypertrophic remodelling.

Lastly, to examine whether increased accumulation of lipotoxic FA metabolites could underlie mitochondrial dysfunction in hearts from ic*Atgl*KO mice, we measured the cardiac content of ceramides and long-chain acyl-CoAs (*Figure 6H* and *I*). Interestingly, cardiac levels of ceramides and long-chain acyl-CoA species were unchanged or decreased in hearts from ic*Atgl*KO mice, suggesting that mitochondrial dysfunction in these hearts was not secondary to increased accumulation of these lipotoxic FA metabolites.

# 4. Discussion

In this study, we tested whether acquired impairment of myocardial TAG catabolism via induced cardiomyocyte-specific ATGL deficiency influences mitochondrial substrate metabolism as well as cardiac structure and function and investigated whether this was associated with impaired PPARα signalling.

As expected, hearts from ic*Atgl*KO mice exhibited a substantial increase in myocardial TAG content that is comparable with that observed in constitutive total*Atgl*KO and muscle*Atgl*KO mice.[28] In addition, hearts from ic*Atgl*KO mice exhibited extensive interstitial fibrosis that was caused by the up-regulation of several genes related to extracellular matrix remodelling. Although increased fibrosis was also observed in hearts from total*Atgl*KO mice,[16] it was unclear whether these effects were a result of ATGL deficiency in cardiomyocytes or other cardiac cell types, such as collagen-producing fibroblasts. Our findings suggest that fibrotic remodelling following ATGL ablation is the result of intercellular signalling from cardiomyocytes to fibroblasts and ensuing up-regulation of profibrotic genes. Since fibrosis can cause increased

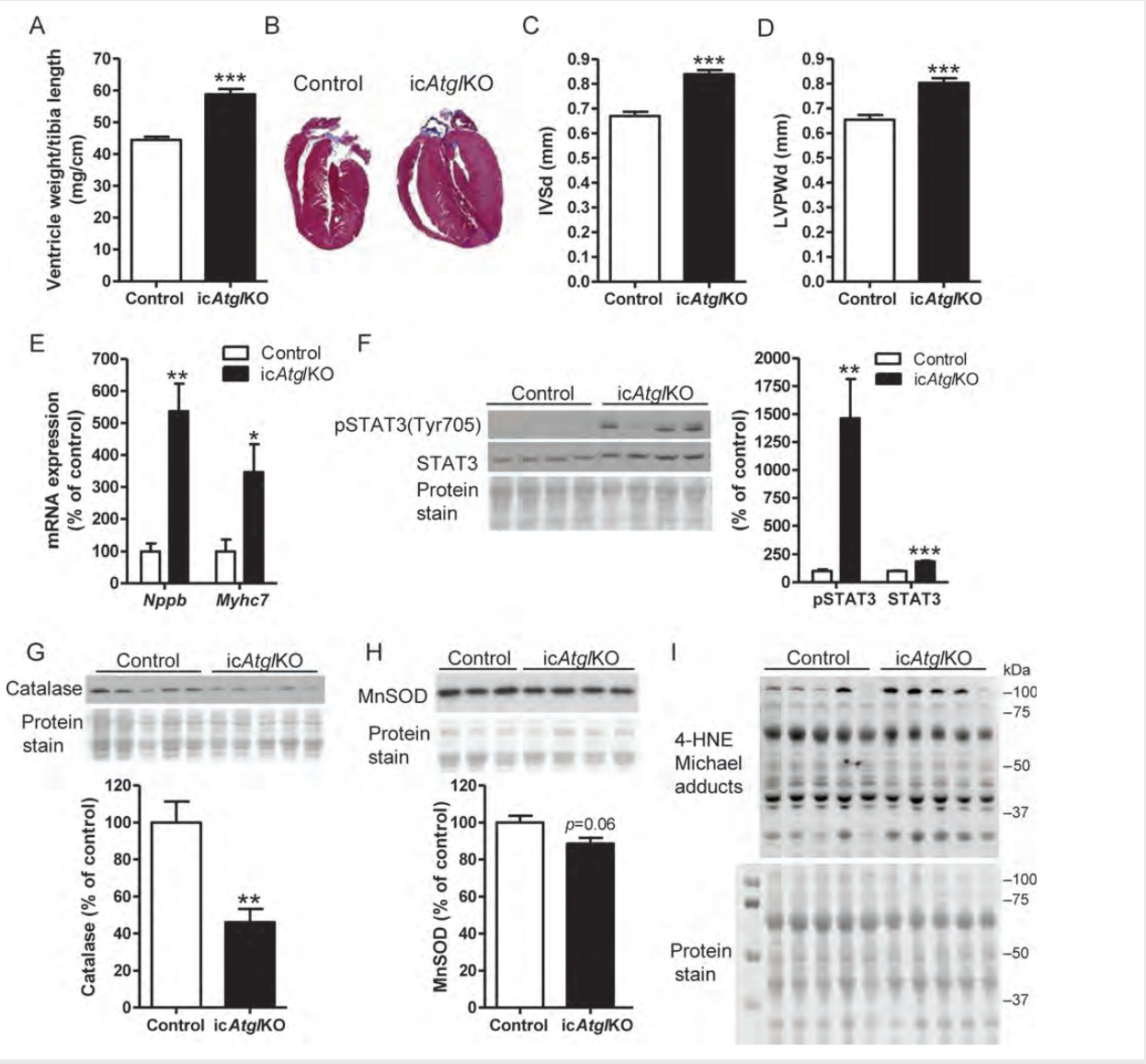


**Figure 4** Analysis of cardiac hypertrophy. (*A*) Ratio of ventricle weight to tibia length (4.5–5.5 weeks *post*-TAM, 4–6-month-old females, $n = 7–13$, $^{***}P < 0.001$). (*B*) Representative M.T.-stained long-axis heart sections (6 weeks *post*-TAM, 8–9-month-old females). (*C*) Echocardiographic assessment of IVSd and (*D*) LVPWd (4 weeks *post*-TAM, 3–6-month-old females, $n = 8–13$, $^{***}P < 0.001$). (*E*) Cardiac mRNA expression of *Nppb* and *Myh7* (5 weeks *post*-TAM, 5–6-month-old males, $n = 4–5$, $^{*}P < 0.05$, $^{**}P < 0.01$). (*F*) Cardiac STAT3 phosphorylation at Tyr705 (ratio of phosphorylated to total STAT3) and protein expression (5 weeks *post*-TAM, 4–5-month-old females, $n = 5$, $^{**}P < 0.01$, $^{***}P < 0.001$). (*G*) Cardiac protein expression of catalase (5 h-fasted, 5.5 weeks *post*-TAM, 8.5-month-old males, $n = 6$, $^{**}P < 0.01$). (*H*) Cardiac protein expression of MnSOD (4 weeks *post*-TAM, 5–6-month-old females, $n = 3–4$). (*I*) Cardiac protein expression of 4-HNE Michael adducts (4 weeks *post*-TAM, 6–7-month-old females).

systolic and diastolic stiffness, our data support the conclusion that increased fibrotic remodelling contributes to cardiac dysfunction in ic*Atgl*KO mice.

Interestingly, hearts from ic*Atgl*KO mice also develop overt pathological hypertrophy. Although the precise mechanisms of hypertrophic remodelling in hearts from ic*Atgl*KO mice require further investigation, it is possible that excessive TAG deposition in cardiomyocytes leads to intracellular mechanical stretch that perturbs the myofibrillar organization, thereby triggering a pro-hypertrophic response to compensate for these adverse changes in myofibril arrangement and function. This notion is supported by the finding that myofibrillar disarray and dysfunction secondary to mutations in sarcomeric proteins are causative for the development of compensatory hypertrophic remodelling in familial hypertrophic cardiomyopathy.[39]

Similar to findings using crude cardiac homogenates from total*Atgl*KO mice,[28] FAO was reduced in working hearts from ic*Atgl*KO mice, which was not compensated by increased glucose oxidation. However, it is possible that the rate of glucose oxidation via TCA cycle anaplerosis is augmented in hearts from ic*Atgl*KO mice, which could not be detected using the perfusion system employed in this study. Indeed, previous studies have demonstrated that hypertrophied hearts exhibit decreased FAO, unchanged glucose oxidation, but increased diversion of glucose-derived pyruvate towards anaplerosis.[40]

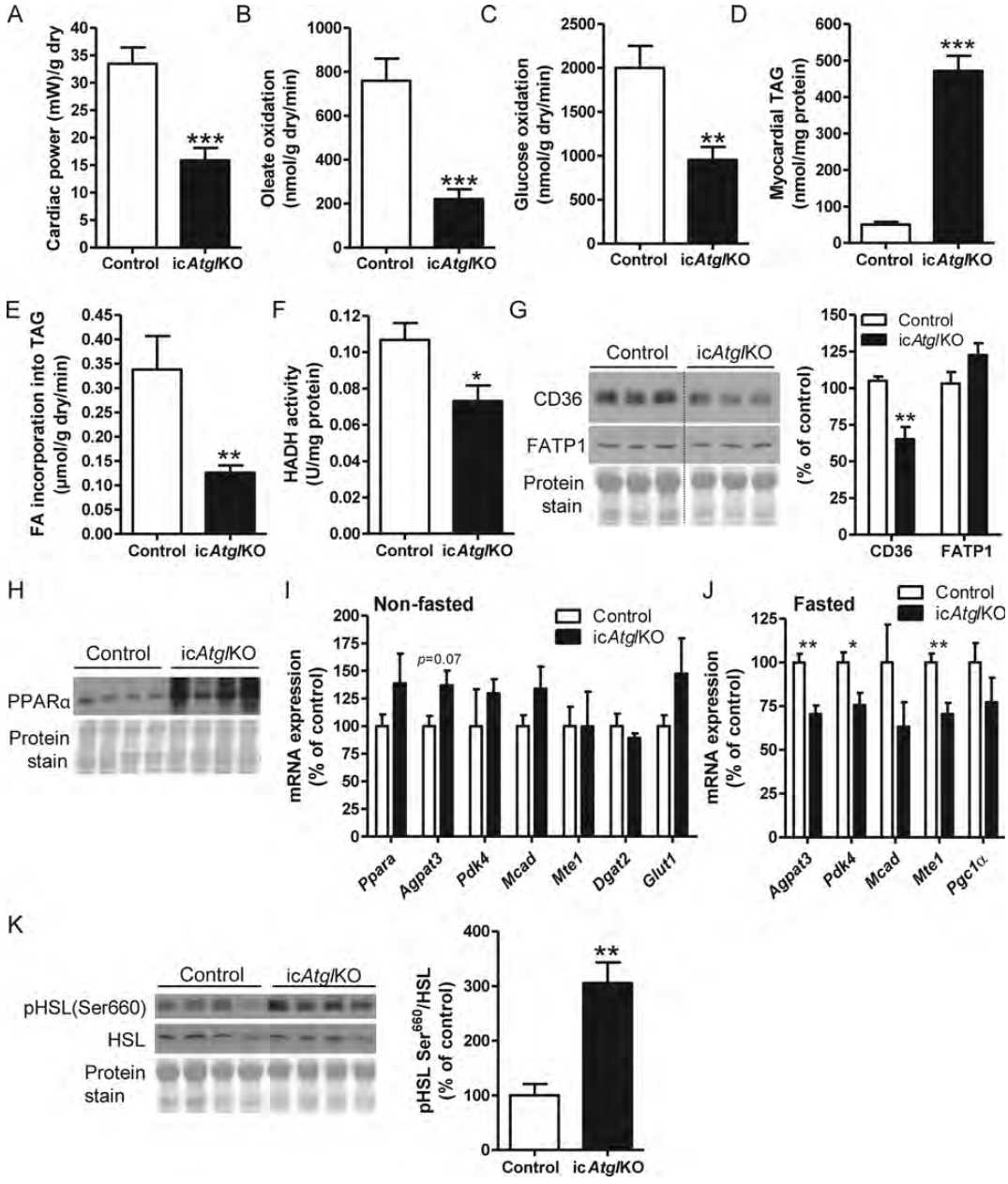


**Figure 5** Myocardial energy metabolism. (*A*) Cardiac power ($n = 9–10$), (*B*) oleate oxidation rates ($n = 9–10$), (*C*) glucose oxidation rates ($n = 9–10$), (*D*) myocardial TAG content ($n = 5–6$), and (*E*) oleate incorporation into TAG ($n = 5–6$) in *ex vivo* perfused working hearts (4–5 weeks *post*-TAM, 6–8-month-old females, $^{**}P < 0.01$, $^{***}P < 0.001$). (*F*) Cardiac HADH activity (4–5 weeks *post*-TAM, 4–5.5-month-old females, $n = 6$, $^{*}P < 0.05$). (*G*) Cardiac CD36 and FATP1 protein expression (4 weeks *post*-TAM, 6-month-old females, $n = 4–6$, $^{**}P < 0.01$). (*H*) Cardiac PPARα protein expression (5 weeks *post*-TAM, 4–5-month-old females). (I and J) mRNA expression of genes involved in FA and glucose metabolism in hearts from (*I*) non-fasted (5 weeks *post*-TAM, 5–6-month-old, $n = 4–5$) and (*J*) 12 h-fasted (4 weeks *post*-TAM, 6.5–7.5-month-old, $n = 5–7$) male mice ($^{*}P < 0.05$, $^{**}P < 0.01$). (*K*) Cardiac HSL phosphorylation at Ser660 (4 weeks *post*-TAM, 6–7-month-old females, $n = 5–6$, $^{**}P < 0.01$).

Interestingly, mRNA expression of PPARα target genes was maintained in hearts from ic*Atgl*KO mice in the non-fasted and short-term (5 h) fasted state and only mildly reduced with prolonged (12 h) fasting. Possible reasons for this milder effect on myocardial PPARα signalling in ic*Atgl*KO mice include differences in background strain (>96.9% C57BL/6 for ic*Atgl*KO vs. pure, >99.91% C57BL/6 for total*Atgl*KO mice, and 93.8–96.9% C57BL/6 for muscle*Atgl*KO mice), the duration of ATGL deficiency (4–6 weeks in ic*Atgl*KO vs. at least 8 weeks and 15–16 weeks, not including time *in utero*, in total*Atgl*KO mice and muscle*Atgl*KO mice, respectively), and the age at the onset of ATGL deficiency (ablation in adult ic*Atgl*KO mice vs. congenital deficiency in total*Atgl*KO and muscle*Atgl*KO mice). Although we cannot exclude the possibility that sufficient residual ATGL activity is still present in hearts from ic*Atgl*KO mice to maintain PPARα signalling at baseline, this is not sufficient to prevent marked cardiac steatosis. However, it is conceivable that up-regulation of HSL activity via increased phosphorylation at Ser660 could partially rescue the effect of ATGL ablation on cardiac TAG accumulation and PPARα signalling.

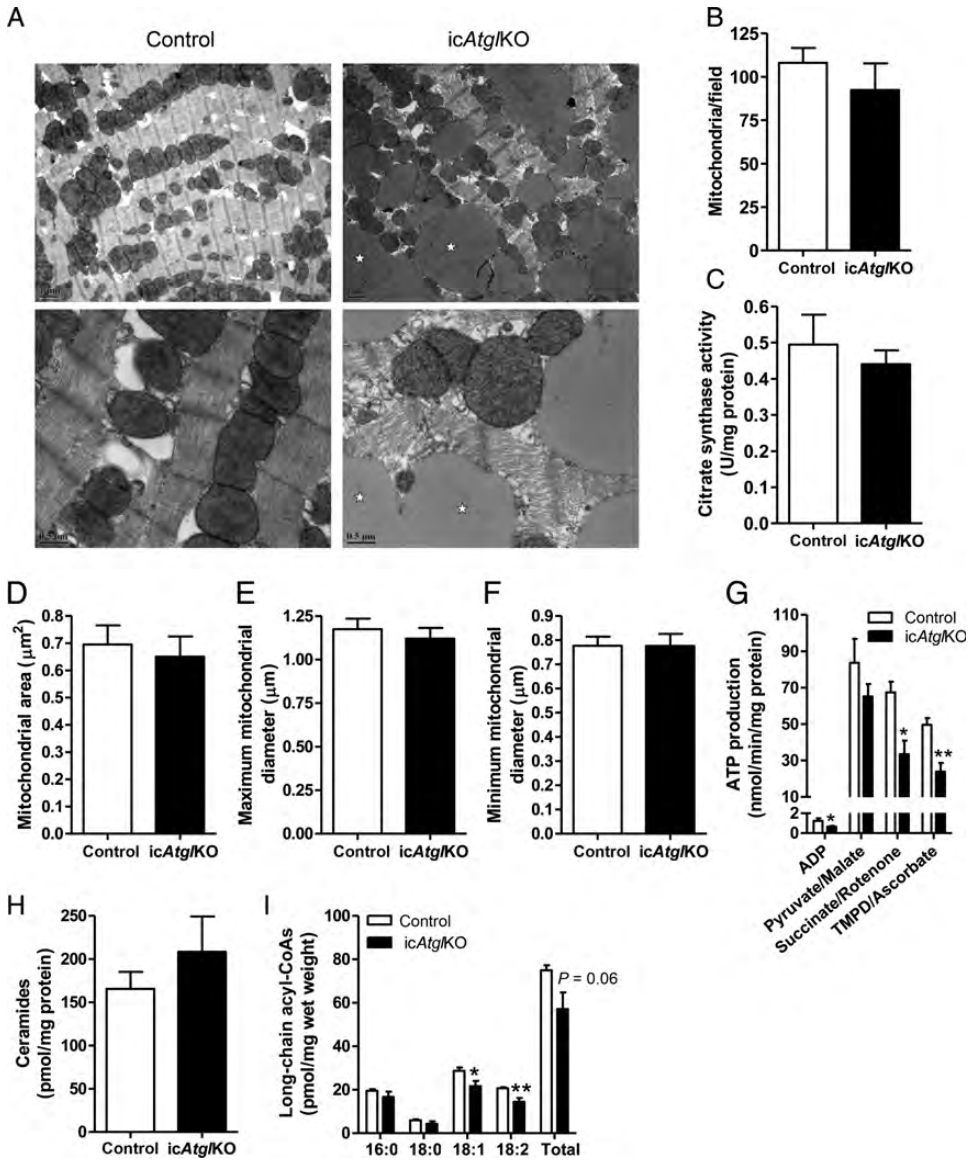


**Figure 6** Mitochondrial analysis. (*A*) Representative electron micrographs of heart sections (4 weeks *post*-TAM, 5.5-month-old females) at ×7100 (upper panel, scale bars denote 1 μm) and ×22000 (lower panel, scale bars denote 0.5 μm) magnification. Stars indicate lipid droplets. (*B*) Mitochondrial number quantified from electron micrographs ($n = 3$ hearts, 5–7 images per heart). (*C*) Cardiac citrate synthase activity (4–5 weeks *post*-TAM, 4–5.5-month-old females, $n = 6$). (*D*) Mitochondrial cross-sectional area, (*E*) maximum and (*F*) minimum mitochondrial diameter ($n = 3$ hearts, 3 sections per heart, 33–46 mitochondria per section). (*G*) Mitochondrial ATP production (6 weeks *post*-TAM, 9-month-old females, $n = 4–5$, $^*P < 0.05$, $^{**}P < 0.01$). (*H*) Cardiac concentrations of ceramides and (*I*) long-chain acyl-CoAs (5 weeks *post*-TAM, 5–6-month-old males, $n = 5$, $^*P < 0.05$, $^{**}P < 0.01$).

It should be noted that cardiac-specific HSL over-expression protected from fasting- and diabetes-induced cardiac steatosis,[41,42] indicating that up-regulation of HSL in hearts from ic*Atgl*KO mice could compensate to some extent for the lack of ATGL. Interestingly, Reilich *et al.*[19] also suggested that β-adrenergic agonist-mediated HSL activation in cells from patients with inactivating *ATGL/PNPLA2* mutations was able to bypass the lipolytic blockade.

PPARα agonist treatment of total*Atgl*KO mice protected from cardiac steatosis, mitochondrial dysfunction, and heart failure.[28] Nonetheless, a beneficial effect of PPARα agonist treatment on cardiac function in humans with *ATGL/PNPLA2* mutations has yet to be demonstrated.[20] Although we have not tested this in the present study, it is likely that over-activation of PPARα via PPARα agonist treatment improves cardiac steatosis and function in ic*Atgl*KO mice by increasing oxidation of FAs taken up into cardiomyocytes in the absence of enhanced TAG catabolism, as has been previously demonstrated using total*Atgl*KO mice.[28]

Regardless of the differences in PPARα signalling between mouse models, the findings of this study suggest that mechanisms other than changes in PPARα signalling also contribute to impaired FAO in hearts from ic*Atgl*KO mice. Consistent with the concept that a significant proportion of FAs in the heart are shuttled through the TAG pool prior to being oxidized in the mitochondria,[1,43] it is likely that a decrease in FAs liberated by TAG hydrolysis may contribute to the reduction in myocardial FAO in ic*Atgl*KO mice. In addition, CD36 protein expression and FA incorporation into the TAG and FFA pool (data not shown) were

decreased in hearts from ic*Atgl*KO mice, suggesting that decreased cardiomyocyte FA uptake via CD36 may also contribute to diminished FAO in the absence of marked changes in PPARα signalling.

In summary, acquired cardiomyocyte-specific ATGL deficiency leads to marked myocardial steatosis, pathological hypertrophy, as well as fibrotic remodelling, which are associated with moderate cardiac dysfunction *in vivo*. Furthermore, mitochondrial FAO is impaired in hearts from ic*Atgl*KO mice, even in the absence of marked changes in cardiac PPARα signalling.

# Supplementary material

Supplementary material is available at *Cardiovascular Research* online.

**Conflict of interest:** none declared.

## Funding

This work was supported by grants from the Canadian Institute of Health Research and the Heart and Stroke Foundation of Canada to J.R.B.D., post-doctoral fellowships from the Heart and Stroke Foundation of Canada and the Canadian Diabetes Association to P.C.K., and Alberta Innovates-Health Solutions post-doctoral fellowships to P.C.K. and T.P., as well as NIH grant R01DK090166 and HHMI ECA grant to E.E.K.

## References

1. Banke NH, Wende AR, Leone TC, O'Donnell JM, Abel ED, Kelly DP *et al*. Preferential oxidation of triacylglyceride-derived fatty acids in heart is augmented by the nuclear receptor PPARalpha. *Circ Res* 2010;**107**:233–241.
2. Kienesberger PC, Pulinilkunnil T, Nagendran J, Dyck JR. Myocardial triacylglycerol metabolism. *J Mol Cell Cardiol* 2013;**55**:101–110.
3. McGavock JM, Lingvay I, Zib I, Tillery T, Salas N, Unger R *et al*. Cardiac steatosis in diabetes mellitus: a 1H-magnetic resonance spectroscopy study. *Circulation* 2007;**116**:1170–1175.
4. McGavock JM, Victor RG, Unger RH, Szczepaniak LS. Adiposity of the heart, revisited. *Ann Intern Med* 2006;**144**:517–524.
5. Marfella R, Di Filippo C, Portoghese M, Barbieri M, Ferraraccio F, Siniscalchi M *et al*. Myocardial lipid accumulation in patients with pressure-overloaded heart and metabolic syndrome. *J Lipid Res* 2009;**50**:2314–2323.
6. Khan RS, Drosatos K, Goldberg IJ. Creating and curing fatty hearts. *Curr Opin Clin Nutr Metab Care* 2010;**13**:145–149.
7. Sharma S, Adrogue JV, Golfman L, Uray I, Lemm J, Youker K *et al*. Intramyocardial lipid accumulation in the failing human heart resembles the lipotoxic rat heart. *Faseb J* 2004;**18**:1692–1700.
8. Christoffersen C, Bollano E, Lindegaard ML, Bartels ED, Goetze JP, Andersen CB *et al*. Cardiac lipid accumulation associated with diastolic dysfunction in obese mice. *Endocrinology* 2003;**144**:3483–3490.
9. Korosoglou G, Humpert PM, Ahrens J, Oikonomou D, Osman NF, Gitsioudis G *et al*. Left ventricular diastolic function in type 2 diabetes mellitus is associated with myocardial triglyceride content but not with impaired myocardial perfusion reserve. *J Magn Reson Imaging* 2012;**35**:804–811.
10. Goldberg IJ, Trent CM, Schulze PC. Lipid metabolism and toxicity in the heart. *Cell Metab* 2012;**15**:805–812.
11. McGavock J, Szczepaniak LS, Ayers CR, Abdullah SM, See R, Gore MO *et al*. The effects of rosiglitazone on myocardial triglyceride content in patients with type 2 diabetes: a randomised, placebo-controlled trial. *Diab Vasc Dis Res* 2012;**9**:131–137.
12. Son NH, Yu S, Tuinei J, Arai K, Hamai H, Homma S *et al*. PPARgamma-induced cardiolipotoxicity in mice is ameliorated by PPARalpha deficiency despite increases in fatty acid oxidation. *J Clin Invest* 2010;**120**:3443–3454.
13. Chokshi A, Drosatos K, Cheema FH, Ji R, Khawaja T, Yu S *et al*. Ventricular assist device implantation corrects myocardial lipotoxicity, reverses insulin resistance, and normalizes cardiac metabolism in patients with advanced heart failure. *Circulation* 2012;**125**:2844–2853.
14. Liu L, Shi X, Bharadwaj KG, Ikeda S, Yamashita H, Yagyu H *et al*. DGAT1 expression increases heart triglyceride content but ameliorates lipotoxicity. *J Biol Chem* 2009;**284**:36312–36323.
15. Liu L, Yu S, Khan RS, Homma S, Schulze PC, Blaner WS *et al*. Diacylglycerol acyl transferase 1 overexpression detoxifies cardiac lipids in PPARgamma transgenic mice. *J Lipid Res* 2012;**53**:1482–1492.
16. Haemmerle G, Lass A, Zimmermann R, Gorkiewicz G, Meyer C, Rozman J *et al*. Defective lipolysis and altered energy metabolism in mice lacking adipose triglyceride lipase. *Science* 2006;**312**:734–737.
17. Hirano K, Ikeda Y, Zaima N, Sakata Y, Matsumiya G. Triglyceride deposit cardiomyovasculopathy. *N Engl J Med* 2008;**359**:2396–2398.
18. Schweiger M, Lass A, Zimmermann R, Eichmann TO, Zechner R. Neutral lipid storage disease: genetic disorders caused by mutations in adipose triglyceride lipase/PNPLA2 or CGI-58/ABHD5. *Am J Physiol Endocrinol Metab* 2009;**297**:E289–E296.
19. Reilich P, Horvath R, Krause S, Schramm N, Turnbull DM, Trenell M *et al*. The phenotypic spectrum of neutral lipid storage myopathy due to mutations in the PNPLA2 gene. *J Neurol* 2011;**258**:1987–1997.
20. van de Weijer T, Havekes B, Bilet L, Hoeks J, Sparks L, Bosma M *et al*. Effects of bezafibrate treatment in a patient and a carrier with mutations in the PNPLA2 gene, causing neutral lipid storage disease with myopathy. *Circ Res* 2013;**112**:e51–e54.
21. Fischer J, Lefevre C, Morava E, Mussini JM, Laforet P, Negre-Salvayre A *et al*. The gene encoding adipose triglyceride lipase (PNPLA2) is mutated in neutral lipid storage disease with myopathy. *Nat Genet* 2007;**39**:28–30.
22. Utz W, Engeli S, Haufe S, Kast P, Hermsdorf M, Wiesner S *et al*. Myocardial steatosis, cardiac remodelling and fitness in insulin-sensitive and insulin-resistant obese women. *Heart* 2011;**97**:1585–1589.
23. Rijzewijk LJ, van der Meer RW, Smit JW, Diamant M, Bax JJ, Hammer S *et al*. Myocardial steatosis is an independent predictor of diastolic dysfunction in type 2 diabetes mellitus. *J Am Coll Cardiol* 2008;**52**:1793–1799.
24. Ng AC, Delgado V, Bertini M, van der Meer RW, Rijzewijk LJ, Hooi Ewe S *et al*. Myocardial steatosis and biventricular strain and strain rate imaging in patients with type 2 diabetes mellitus. *Circulation* 2010;**122**:2538–2544.
25. Szczepaniak LS, Victor RG, Orci L, Unger RH. Forgotten but not gone: the rediscovery of fatty heart, the most common unrecognized disease in America. *Circ Res* 2007;**101**:759–767.
26. Szczepaniak LS, Dobbins RL, Metzger GJ, Sartoni-D'Ambrosia G, Arbique D, Vongpatanasin W *et al*. Myocardial triglycerides and systolic function in humans: *in vivo* evaluation by localized proton spectroscopy and cardiac imaging. *Magn Reson Med* 2003;**49**:417–423.
27. van der Meer RW, Rijzewijk LJ, Diamant M, Hammer S, Schar M, Bax JJ *et al*. The ageing male heart: myocardial triglyceride content as independent predictor of diastolic function. *Eur Heart J* 2008;**29**:1516–1522.
28. Haemmerle G, Moustafa T, Woelkart G, Buttner S, Schmidt A, van de Weijer T *et al*. ATGL-mediated fat catabolism regulates cardiac mitochondrial function via PPAR-alpha and PGC-1. *Nat Med* 2011;**17**:1076–1085.
29. Kienesberger PC, Lee D, Pulinilkunnil T, Brenner DS, Cai L, Magnes C *et al*. Adipose triglyceride lipase deficiency causes tissue-specific changes in insulin signaling. *J Biol Chem* 2009;**284**:30218–30229.
30. Huang TT, Naeemuddin M, Elchuri S, Yamaguchi M, Kozy HM, Carlson EJ *et al*. Genetic modifiers of the phenotype of mice deficient in mitochondrial superoxide dismutase. *Hum Mol Genet* 2006;**15**:1187–1194.
31. Kienesberger PC, Pulinilkunnil T, Sung MM, Nagendran J, Haemmerle G, Kershaw EE *et al*. Myocardial ATGL overexpression decreases the reliance on fatty acid oxidation and protects against pressure overload-induced cardiac dysfunction. *Mol Cell Biol* 2012;**32**:740–750.
32. O'Connell TD, Rodrigo MC, Simpson PC. Isolation and culture of adult mouse cardiac myocytes. *Methods Mol Biol* 2007;**357**:271–296.
33. Boudina S, Sena S, O'Neill BT, Tathireddy P, Young ME, Abel ED. Reduced mitochondrial oxidative capacity and increased mitochondrial uncoupling impair myocardial energetics in obesity. *Circulation* 2005;**112**:2686–2695.
34. Tasseva G, Bai HD, Davidescu M, Haromy A, Michelakis E, Vance JE. Phosphatidylethanolamine deficiency in Mammalian mitochondria impairs oxidative phosphorylation and alters mitochondrial morphology. *J Biol Chem* 2013;**288**:4158–4173.
35. Tsai JY, Kienesberger PC, Pulinilkunnil T, Sailors MH, Durgan DJ, Villegas-Montoya C *et al*. Direct regulation of myocardial triglyceride metabolism by the cardiomyocyte circadian clock. *J Biol Chem* 2010;**285**:2918–2929.
36. Pinent M, Hackl H, Burkard TR, Prokesch A, Papak C, Scheideler M *et al*. Differential transcriptional modulation of biological processes in adipocyte triglyceride lipase and hormone-sensitive lipase-deficient mice. *Genomics* 2008;**92**:26–32.
37. Benjamini Y, Hochberg Y. Controlling the False Discovery Rate: A Practical and Powerful Approach to Multiple Testing. *J R Statist Soc B* 1995;**57**:289–300.
38. Pulinilkunnil T, Kienesberger PC, Nagendran J, Waller TJ, Young ME, Kershaw EE *et al*. Myocardial adipose triglyceride lipase overexpression protects diabetic mice from the development of lipotoxic cardiomyopathy. *Diabetes* 2013;**62**:1464–177.
39. Bashyam MD, Savithri GR, Kumar MS, Narasimhan C, Nallari P. Molecular genetics of familial hypertrophic cardiomyopathy (FHC). *J Hum Genet* 2003;**48**:55–64.
40. Sorokina N, O'Donnell JM, McKinney RD, Pound KM, Woldegiorgis G, LaNoue KF *et al*. Recruitment of compensatory pathways to sustain oxidative flux with reduced carnitine palmitoyltransferase I activity characterizes inefficiency in energy metabolism in hypertrophied hearts. *Circulation* 2007;**115**:2033–2041.
41. Ueno M, Suzuki J, Zenimaru Y, Takahashi S, Koizumi T, Noriki S *et al*. Cardiac overexpression of hormone-sensitive lipase inhibits myocardial steatosis and fibrosis in streptozotocin diabetic mice. *Am J Physiol Endocrinol Metab* 2008;**294**:E1109–E1118.
42. Suzuki J, Shen WJ, Nelson BD, Patel S, Veerkamp JH, Selwood SP *et al*. Absence of cardiac lipid accumulation in transgenic mice with heart-specific HSL overexpression. *Am J Physiol Endocrinol Metab* 2001;**281**:E857–E866.
43. Saddik M, Lopaschuk GD. Myocardial triglyceride turnover and contribution to energy substrate utilization in isolated working rat hearts. *J Biol Chem* 1991;**266**:8162–8170.